Comparison of New Element Designs For Combined RF-Shim Arrays at 7T

Simone Angela Winkler[1], Jason P Stockmann[2], Paul A Warr[3], Boris Keil[2], Lawrence L Wald[2,4], and Brian K Rutt[1]

[1]*Dept. of Radiology, Stanford University, Stanford, CA, United States,* [2]*A. A. Martinos Center for Biomedical Imaging, Massachusetts General Hospital, Harvard Medical School, Charlestown, Massachusetts, United States,* [3]*Department of Electrical & Electronic Engineering, University of Bristol, Clifton, United Kingdom,* [4]*Harvard-MIT Health Sciences and Technology, Massachusetts Institute of Technology, Cambridge, Massachusetts, United States*

Target Audience: MR engineers and physicists with an interest in RF and B_0 shim array concepts.

Purpose: To identify novel concepts for RF-shim loop architectures suitable for 7T, and to determine their relative SNR performance.

Background: Higher order B_0 shimming of the brain is an essential tool for modern MR neuroimaging, as B_0 inhomogeneities cause significant artifacts, especially at ultra high field strengths such as 7T. Multi-coil shimming has recently been proposed as a more efficient, less expensive alternative to spherical harmonic shim coils[1]. In the initial realization for brain shimming at 7T, multi-coil multi-row shim arrays were placed near the top and bottom of the head with a gap in between for the RF Tx/Rx coil. The disadvantage of this approach is that it restricts the space available for RF arrays, such as massively parallel receive arrays, and potentially interferes with RF performance. To overcome this problem, it has been proposed that multi-coil shim loops share the same helmet as receive-only RF loops in close proximity to the head, optimizing the efficiency of both systems. The integration of both RF receive and B_0 shim function onto the same loop conductors at 3T has been recently reported[2,3]. The published implementations use toroidal RF chokes to bridge each capacitor in order to create a DC path around each receive loop (Fig. 1b). However, at 7T, a larger number of capacitors and thus chokes would be required, thereby introducing additional loss, heating, RF field perturbation, bulk and construction complexity. Additionally, the added DC-shim wiring can potentially cause perturbation of the RF signal causing potential SNR loss. This abstract reports on the analysis of several approaches for incorporating B_0 shimming functionality into receive-only RF elements, with particular focus on suitability at 7T and the maintenance of SNR performance. We investigated two new loop designs. The first approach uses coaxial cable for loop construction, with the inner conductor carrying the shim current, and the outer acting as the RF resonant loop (Fig 1c). The second involves concentric coplanar loops with the inner carrying the shim current (Fig. 1d).

Fig. 1 Proposed RF-shim loop geometries (a) conventional loop, (b) RF-shim loop with chokes, (c) coaxial loop, (d) concentric loop.

Theory: Magnetic coupling between the two loops in the new RF-shim topologies results in a field system comprising two conjugate poles and two conjugate zeroes, i.e. a resonance and an anti-resonance. The frequency of the resonance is related to that of the stand-alone RF loop by $(1-k^2)^{-0.5}$, k =inter-loop coupling factor. The resulting reduction in Q factor accounts for the SNR trend with k. The frequency of the anti-resonance is related to that of the resonance of the stand-alone RF loop by $(1+\alpha)^{-0.5}$, $\alpha = \sqrt{\frac{L_S}{L_{RF}} - \frac{2L_m}{L_{RF}}}$, L_s = shim loop inductance, L_{RF} = RF loop inductance and L_m = mutual inductance between the two loops. Around both resonance and anti-resonance frequencies, the current in the shim loop is antiphase to that in the RF loop. The variation in Q factor was used to confirm SNR prediction for loops with varying coupling factors.

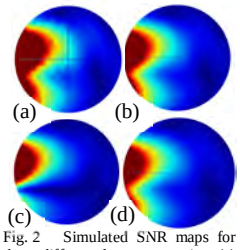

Fig. 2 Simulated SNR maps for three different loop geometries: (a) conventional, (b) established RF-shim, (c) coaxial loop, (d) concentric loop.

Methods: We compared four loop types: the conventional RF loop without shim function, the established 3T approach of chokes shunting the loop capacitors, a coaxial loop, and a concentric loop (Figs. 1 a-d, respectively). All loops were constructed with 45 mm RF loop radius. Loops a, b, and d were constructed from AWG-16 tin-coated copper wire, loop c was made from Microcoax UTiFORM RG-141 coaxial cable. All loops were tuned to 298 MHz. We simulated the SNR performance of the three RF-shim loop types using COMSOL (COMSOL, Inc., Burlington, MA, USA) and a spherical phantom model of 10 cm radius (ε_r = 78, σ = 0.8 S/m). A parametric study was carried out, in which the distance between RF and shim conductors was varied for the concentric type, and coax types RG-085, RG-141, and RG-250 were used for the coaxial type (other arbitrary coaxial cable dimensions as listed in Table I were also analyzed as reported below). Simulated SNR was defined as B_1^- divided by the square root of total sample loss power and was then averaged over a relevant ROI and referenced against the same quantity simulated for the RF-only loop. We also obtained experimental SNR maps using single loops of all four loop types, on a 7T Siemens scanner (Siemens Healthcare, Erlangen, Germany) using a realistic head/brain phantom located 1.25 cm from the coil plane, and with brain compartment electric properties as follows: ε_r = 78, σ = 0.8 S/m (Fig. 3). The SNR maps were obtained with a FLASH sequence with the flip angle set to 90 degrees near the edge of the phantom and were averaged over an ROI comparable to simulation. Optimal SNR was calculated using the method described by [Kellman2005] and then averaged over an ROI comparable to the simulations.

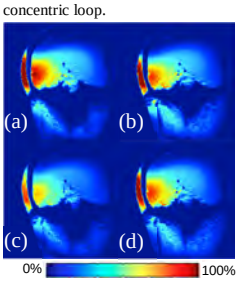

Fig. 3 Experimental SNR maps for the four loop types.

Results: Simulated and experimental SNR maps are shown in Figs. 2 and 3, respectively. The RF-shim loop with chokes exhibited an average SNR of 81% in simulation and 85% in experiment (all SNR values referenced to that of the conventional RF loop without added shim function). The RG-141 coaxial loop exhibited an average SNR of 58% in simulation and 72% by experiment, whereas the concentric loop with 30 mm shim loop radius showed average SNR of 71% in simulation and 88% by experiment. The parametric study results are shown in Table I. In all cases, we observe larger SNR values for larger separations between RF and shim conductors, which can be attributed to the reduced coupling between the conductors and thus increased Q ratio as predicted by the coupling factor k in our analytical formulation.

TABLE I
RELATIVE SNR FOR DIFFERENT LOOP TYPES

Loop type		Parameters		Rel. SI
Conventional				100%
		r_{loc} (mm)		
Concentric		30		71%
		32		70%
		34		68%
		36		66%
		38		63%
		40		62%
		42		58%
		r_{shield} (mm)	r_{inner} (mm)	
Coaxial	RG-250	6.3	1.5	64%
	RG-141	3.0	0.9	58%
	RG-085	2.0	0.6	53%
		6.3	0.6	71%
		6.3	0.9	67%
		3.0	0.6	63%
		3.0	1.5	56%
		2.0	0.9	52%
		2.0	1.5	48%

Discussion and Conclusion: All RF-shim loop types exhibit some loss in SNR. Experimentally, the coaxial type showed the largest SNR drop; however, it also offers a number of advantages: a) inherent coupling raises the resonant frequency and reduces the number of required capacitors; b) no chokes needed; c) reduced sensitivity to shim wires; d) ease of construction. By comparison, the concentric loop has advantages of a) less SNR degradation as compared to the coaxial loop; and b) more flexibility for conductor spacing; however, it suffers from increased construction complexity. In summary, the concentric loop with sufficiently small inner loop diameter, as well as the coaxial loop with sufficiently large ratio of outer to inner conductor radii, both provide viable solutions for RF-shim loop architectures at 7T. In future work the performance of each element type will be characterized in the array environment.

References: [1]Juchem C, JMR 2011, [2]Truong TK, NeuroImage 2014, [3]Stockmann ISMRM 2014, p. 400. [4]Kellman P, MRM 2005.

Acknowledgement: Research support from BWF, NSERC, NIH (P41 EB015891, 1 S10 RR026351-01Al, and R21EB017338), and GE Healthcare.